J Mater Sci: Mater Med (2008) 19:2971–2981
DOI 10.1007/s10856-008-3409-2

Development and bio-electrochemical characterization of a novel TiO_2–SiO_2 mixed oxide coating for titanium implants

S. M. A. Shibli · Suja Mathai

Received: 16 November 2007 / Accepted: 19 February 2008 / Published online: 24 March 2008

Abstract Titanium and its alloys, the most commonly used materials for dental and orthopaedic implants are generally coated with bioactive materials such as sol–gel derived titania, silica and calcium phosphate in order to render these materials bioactive. In the present work a coating containing nanosized titania particles having anatase structure was developed on titanium substrate by thermal decomposition of titanium tetrachloride in isopropanol. A modified titania–silica mixed oxide coating was developed by incorporating the required amount of silica in the coating system. The presence of silica at small weight percentage caused improvement of adhesion and corrosion resistance of the coating. In vitro bioactivity tests were performed in 1.5 Kokubo's simulated body fluid after alkaline treatment of the titania/titania–silica coatings and the performance was compared with that of the titania coating developed by simple thermal oxidation. TF-XRD, FTIR and SEM-EDAX were used to investigate the microstructural morphology and crystallinity of the coatings. Elemental analysis of simulated body fluid was carried out using ICP-AES and spectrophotometry. Enhanced biogrowth was facilitated on the titania coating incorporated with low silica content.

1 Introduction

Commercially available pure titanium (Ti) is the most commonly used material for dental and orthopaedic implants because of its excellent biocompatibility, corrosion resistance and adequate load-bearing properties [1, 2]. The biocompatibility of Ti as an implant material is attributed to surface oxides spontaneously formed in air and/or physiological fluids [3, 4]. The surface oxides are amorphous and are only few nanometers in thickness. As a result the implants may lose its surface protective layer in long term, particularly submitted to fretting. In addition Ti and its alloys do not bond to bone in the early (<6 months) post-implantation stage [5]. The integration with bone tissue can be improved and accelerated by the presence of a calcium phosphate (CaP) especially hydroxyapatite (HAp), $Ca_{10}(PO_4)_6(OH)_2$ with a similar chemical composition and crystallographic structure as that of bone onto the metal implant surface [6]. It is difficult to achieve a firm bonding between CaP, primarily HAp and Ti, because their crystal structures and thermal expansion coefficients are quite different [7].

The presence of an intermediate layer is thought to be significant to influence chemical bonding between an HAp coating and a substrate [7]. Titanium dioxide (TiO_2) has gained much interest as a coating system on Ti. The bioactivity of TiO_2 microspheres and sol–gel derived titania films have been investigated. The bioactive materials can initiate CaP in situ in the physiological environment. The CaP is more suitable for the target tissue, since the physiological environment directly influences its formation and also that the crystal size of the in situ formed CaP corresponds to that of bone apatite crystals [8]. Thick coatings of TiO_2 can be applied on surgical implants by plasma spray at high temperatures [9, 10]. The plasma spray deposition technique suffers certain disadvantages that it is a line-of-sight process which produce a non-uniform coating when applied to porous and non-regular substrates, because of the high temperature involved, this technique has also the potential of altering the fatigue properties of Ti implants.

S. M. A. Shibli (✉) · S. Mathai
Department of Chemistry, University of Kerala, Kariavattom Campus, Thiruvananthapuram, Kerala 695 581, India
e-mail: smashibli@yahoo.com

Lin CM et al. developed a TiO_2–HAp double layer coating on Ti in which TiO_2 pre-layer coating on Ti was carried out by electrolytic deposition of titanium tetrachloride ($TiCl_4$)/ethanol system [11]. These TiO_2–HAp double-layered coatings showed more adhesion and bioactivity than the single HAp coating on Ti in SBF. The cell activity assay indicated that both the developed coatings are non-toxic to the cells. In the present work nanosized anatase form of TiO_2 coatings were developed on Ti by thermal decomposition of $TiCl_4$/isopropanol at 500°C [12]. The effect of silica (SiO_2) content in the coating system was evaluated by various physicochemical, electrochemical and bioactivity studies. The presence of SiO_2 in the coating enhanced the adhesion and bioactivity. The results are discussed in this article.

2 Materials and methods

2.1 Materials preparation

Titanium tetrachloride, $TiCl_4$ (Spectrochem, assay 99%) and pure silica, SiO_2 powders (Chemplast, assay 99.9%) were used. Mixtures of the following compositions in isopropanol solution were prepared as (a) 100 wt.% TiO_2 + 0 wt.% SiO_2 (b) 90 wt.% TiO_2 + 10 wt.% SiO_2, and (c) 80 wt.% TiO_2 + 20 wt.% SiO_2. Commercially available pure Ti specimens (Grade T3160) of area 2 × 1 cm^2 and 1mm thickness were used as the substrate for the coating. They were mechanically polished using 36-grit SiC paper, rinsed with water followed by ethanol and then with acetone for 15 min each. They were etched in a mixture of 2 ml HF (40%) and 4 ml HNO_3 (66%) in 1,000 ml water for 10 min to form a fresh TiO_2 surface [13]. The specimens were fixed in a mandrel. The $TiCl_4$–SiO_2 mixed solution was applied on the specimens by simply brushing and dried at 80°C for 30 min. This process was repeated successively on all the coatings. Finally the coatings were subjected to firing in a muffle furnace for 1 h. The total wt.% of the mixed oxides/cm^2 was fixed as 10 mg. The parameters such as the quantity of the solution applied, drying temperature, firing temperature, firing time, etc., were optimized during preliminary studies. Another TiO_2 coating was also developed on bare Ti by thermal oxidation at 500°C for 1 h in a muffle furnace. The performances of the TiO_2 and TiO_2–SiO_2 mixed oxide coatings developed by thermal decomposition were compared also with that of the TiO_2 coating developed by thermal oxidation (T.O TiO_2).

2.2 Surface characterization

The adhesion of the TiO_2 and TiO_2–SiO_2 oxide coatings on Ti was determined by performing bend test. Bend test was done by bending the plates through an angle of 180°. After bending the deformed area of the plates was examined by peeling or flaking of the coating from the substrates by a magnifying lens, which indicate poor adhesion. The wear resistance of the oxide coatings was examined by rubbing the plates with abrasive papers of different grades. The porosity of the coatings was compared by applying a ferroxyl reagent on the surface of the coatings [14]. Hardness was measured using a Vicker's microhardness indenter as per ASTM-E 384-05 using an instrument of Shimadzu HMV2000. A load of 25 gfw for 14 s was applied for indentation. The morphology of the coatings before and after electrochemical (anodic polarization) tests was analyzed using an optical microscope (Olympus sz61, magnification ×40). The morphology of the coatings before and after bioactivity study was analyzed microscopically using a scanning electron microscope (SEM) (JEOL-JSM-840A) coupled with energy dispersive X-ray analysis (EDAX). The phases of the coatings were analyzed using a thin film X-ray diffractometer (TF-XRD) (model: X-Pert Pro). In the TF-XRD measurements CuKα radiation at 40 KV and 30 mA was used as the X-ray source and the samples were scanned from 10° to 70° 2θ at a scan rate of 1.2° min^{-1}. The structural analysis of the coatings was carried out based on Fourier transform infrared (FTIR) spectroscopy (Shimadzu FTIR spectrophotometer, Model: IRPrestige-21).

2.3 Electrochemical evaluation

The electrochemical behavior of the TiO_2 and TiO_2–SiO_2 mixed oxide coatings in 0.9% NaCl solution and Hank's balanced salt solution (HBSS) were studied. The composition of the ions in mmol/l of the HBSS was Na^+: 142.0, K^+: 5.81, Mg^{2+}: 0.898, Ca^{2+}: 1.26, Cl^-: 146.0, HCO_3^-: 4.17, HPO_4^{2-}: 0.779 and SO_4^{2-}: 0.406. The HBSS was prepared by dissolving the required amount of reagent-grade chemicals of NaCl, $NaHCO_3$, KCl, KH_2PO_4, $MgCl_2 \cdot 6H_2O$, $MgSO_4 \cdot 7H_2O$, $CaCl_2 \cdot H_2O$, Na_2HPO_4 and D-glucose in distilled water [15, 16]. Both the solutions were kept at 36.5°C.

The open circuit potential (OCP), i.e., the equilibrium potential of the electrode surface without any external electrical contact of the TiO_2 and TiO_2–SiO_2 mixed oxide coatings was monitored with reference to a saturated calomel electrode using a digital multimeter (SYSTRONICS 437T). Potentiodynamic polarization measurements at OCP were recorded after 60 min of immersion of the coated specimen in the physiological solutions. During the measurement the solution was deaerated by bubbling with high purity nitrogen gas.

The electrochemical impedance measurements were carried out using an instrument of Autolab PGSTAT 30

with FRA2 electrochemical system. An Ag/AgCl and a platinum foil were used as reference and auxiliary electrodes. The TiO_2/TiO_2–SiO_2-coated specimen was used as working electrode. The measurements were made at OCP after 30 min of immersion in physiological solutions at 25°C. The measurements were made in frequency range from 1 MHz to 0.1 Hz and sampling with a frequency of 10 points per decade. Using software of Autolab FRA2 performed the data acquisition and analysis.

2.4 Evaluation of bioactivity

Based on preliminary studies the wt.% of SiO_2 to be added into the $TiCl_4$/isopropanol system was optimized. Three different coating systems, i.e., the TiO_2 coating obtained by thermal oxidation, the 100 wt.% TiO_2 coating and the TiO_2–SiO_2 mixed oxide coating containing optimum wt.% of TiO_2 and SiO_2 were chosen for alkaline treatment in 5 M NaOH at 60°C for 24 h followed by biomimetic growth in Kokubo's 1.5 simulated body fluid (SBF) for 14 days at 36.5°C. The specimens were then soaked in 10 mL of an acellular simulated body fluid (1.5 SBF) of composition Na^+: 213.0, K^+: 7.5, Mg^{2+}: 2.3, Ca^{2+}: 3.8, Cl^-: 221.7, HCO_3^-: 221.7, HPO_4^{2-}: 6.3, SO_4^{2-}: 0.8 mmol/l at 36.5°C and pH 7.4. A 1.5 SBF solution was prepared by dissolving the required amount of reagent-grade chemicals of NaCl, $NaHCO_3$, KCl, $K_2HPO_4 \cdot 3H_2O$, $MgCl_2 \cdot 6H_2O$, $CaCl_2$, and Na_2SO_4 in distilled water and buffered to pH 7.4 using a solution of tris-hydroxymethyl aminomethane ($(CH_2OH)_3CNH_2$) and 1.0 M HCl [17]. The ratio of specimen surface area to soaking solution volume, S/V was 0.05 cm^{-1} [18]. The surface potential change during biomimetic growth was monitored out by OCP measurements.

3 Results

3.1 Surface characterization

The results of micro-hardness, thickness, porosity and wear resistance of the TiO_2 and TiO_2–SiO_2 coatings are shown in Table 1. The adhesive strength was evaluated relatively and there was a loss in adhesive strength of the TiO_2–SiO_2 coatings when higher wt.% of SiO_2 was incorporated. The coating of 90 wt.% TiO_2 + 10 wt.% SiO_2 exhibited good adhesion on Ti and there was no peeling or surface blemishing during bend test through an angle of 180°. Wear is defined as the change to a solid surface and a contacting substance. The wear resistance of the TiO_2–SiO_2 coatings were found to be better than that of the 100 wt.% TiO_2 coating. The coating thickness was in the range of 10–13 μm. In the present work, the extent of porosity was quantified relatively with respect to the percentage area of colouration for a definite time from the application of the reagent during the ferroxyl test. The blue spots developed during ferroxyl reagent test revealed that the TiO_2–SiO_2 mixed oxide coating developed by thermal decomposition was porous in nature. The Vicker's microhardness value decreased with increasing SiO_2 content in the TiO_2–SiO_2 mixed oxide coatings.

3.2 Electrochemical evaluation

The trend of OCP variation in 0.9% NaCl and HBSS of the TiO_2 coatings developed by thermal oxidation, the 100 wt.% TiO_2 and the TiO_2–SiO_2 mixed oxide coatings developed by thermal decomposition are shown in Fig. 1a and b. All the coatings showed a cathodic shift for 10 days and then the potential became steady. Both the uncoated Ti and 90 wt.% TiO_2 + 10 wt.% SiO_2 coating exhibited more anodic behavior in the physiological solutions. The cathodic behavior was more pronounced for the TiO_2–SiO_2 mixed oxide coating having higher wt.% of SiO_2. The variations in the OCP values were found to be less than 10 mV in any case.

The anodic polarization behavior in 0.9% NaCl and HBSS of the TiO_2 coatings developed by thermal oxidation, 100 wt.% TiO_2 and the TiO_2–SiO_2 mixed oxide coatings developed by thermal decomposition are shown in Fig. 2a and b. All the coatings could withstand at a current density of 50 mA/cm^2. There were variations of less than 2 mA in the current values. There was no detachment or decohesion of the coatings from the substrate as evidenced from the optical micrographs of the coatings recorded before and after polarization (figures not shown). The 90 wt.% TiO_2 + 10 wt.% SiO_2 coating showed a lower

Table 1 Physical characteristics of TiO_2–SiO_2 coatings on Ti substrate

S. no.	Wt.% of TiO_2–SiO_2 on Ti substrate	Physical characteristics			
		Microhardness	Thickness (μm)	Porosity	Wear resistance
1	T.O TiO_2	156 ± 12.7	–	Generally porous	Fair
2	100 wt.% TiO_2 + 0 wt.% SiO_2	14.72 ± 1.84	10	Porous	Fair
3	90 wt.% TiO_2 + 10 wt.% SiO_2	12.56 ± 1.22	12	More porous	Good
4	80 wt.% TiO_2 + 20 wt.% SiO_2	11.84 ± 1.38	13	Still more porous	Fair

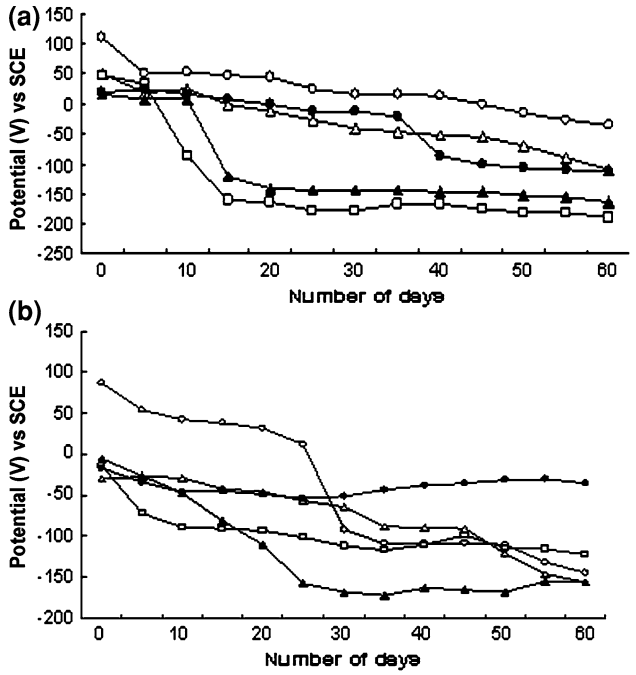

Fig. 1 OCP variation with time of TiO_2 and TiO_2–SiO_2 coatings on Ti (○, uncoated Ti; △, T.O TiO_2; □, 100 wt.% TiO_2 + 0 wt.% SiO_2; ●, 90 wt.% TiO_2 + 10 wt.% SiO_2; ▲, 80 wt.% TiO_2 + 20 wt.% SiO_2) in (**a**) 0.9% NaCl and (**b**) HBSS at pH 7.4 and 36.5°C

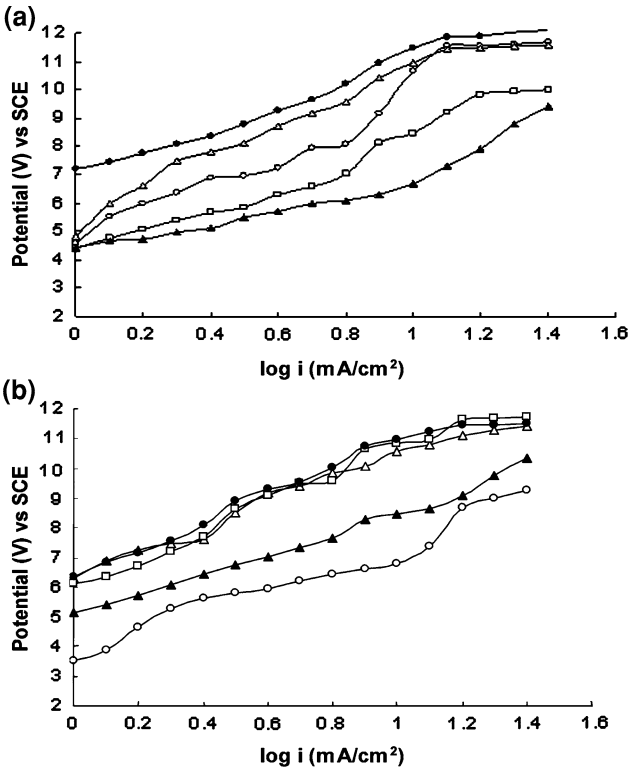

Fig. 2 Potentiodynamic polarization curves of TiO_2 and TiO_2–SiO_2 coatings on Ti (○, uncoated Ti; △, T.O TiO_2; □, 100 wt.% TiO_2 + 0 wt.% SiO_2; ●, 90 wt.% TiO_2 + 10 wt.% SiO_2; ▲, 80 wt.% TiO_2 + 20 wt.% SiO_2) in (**a**) 0.9% NaCl and (**b**) HBSS at pH 7.4 and 36.5°C

current density for higher applied potential in both the physiological solutions, which revealed relatively high corrosion resistance of the coating.

The Nyquisite plots (combined) in 0.9% NaCl and HBSS of the TiO_2 coatings developed by thermal oxidation, the 100 wt.% TiO_2 and the TiO_2–SiO_2 mixed oxide coatings developed by thermal decomposition are shown in Fig. 3a and b. The two-layer model for the TiO_2 and TiO_2–SiO_2 mixed oxide coatings on Ti are shown in Fig. 4a. On examining the Nyquisite plots it was found that the TiO_2 and TiO_2–SiO_2 mixed oxide coating exhibited an inductance type impedance curve. The spectra were interpreted in terms of an "equivalent circuit" with the circuit elements representing electrochemical parameters. Figure 4b shows the equivalent circuit used for fitting the spectra obtained for the coatings in 0.9% NaCl and HBSS. R_s is the resistance of the solution, 0.9% NaCl or HBSS, R_{pL} and C_{pL} are the resistance of the porous layer with the electrolyte inside the pores and the capacitance of the porous layer, respectively. R_{bL} and C_{bL} are the resistance and capacitance of the barrier layer, respectively. The quality of fitting to the equivalent circuit was judged by the χ^2-value. The results of this fitting are presented in Table 2. The obtained values of χ^2 indicate a good fitting to the proposed circuit. In this study a constant phase element (CPE) instead of an ideal capacitor was used for data adjustment. The impedance of the CPE is given by $Z_{CPE} = C\{(j\omega)^n\}^{-1}$, where C is the capacitance associated to an ideal capacitor, ω is the angular frequency and $-1 < n < 1$, when $n = 1$, CPE is an ideal capacitor. The n-value greater than 1 could reveals the deviation from the ideal capacitive behavior [19].

3.3 Evaluation of bioactivity

The stability of the oxides depends strongly on the composition, structure, and thickness of the layer formed. The biological response also depends on the chemical composition of the coating applied on Ti substrate [3]. The wt.% of SiO_2 to be added into the $TiCl_4$/isopropanol system was optimized. The TiO_2 coating obtained by thermal oxidation, 100 wt.% TiO_2 coating and TiO_2–SiO_2 mixed oxide coating containing optimum wt.% of TiO_2 and SiO_2 were chosen for biomimetic growth in Kokubo's 1.5 simulated body fluid.

The surface potential change occurred on the TiO_2 and TiO_2–SiO_2 mixed oxide coatings during biomimetic growth in 1.5 SBF was monitored for 7 days and the potential changes are shown in Fig. 5. The surface potential was highly negative at the beginning in the SBF. The potential shifted to move in anodic direction and attained a maximum positive value within a few days and then

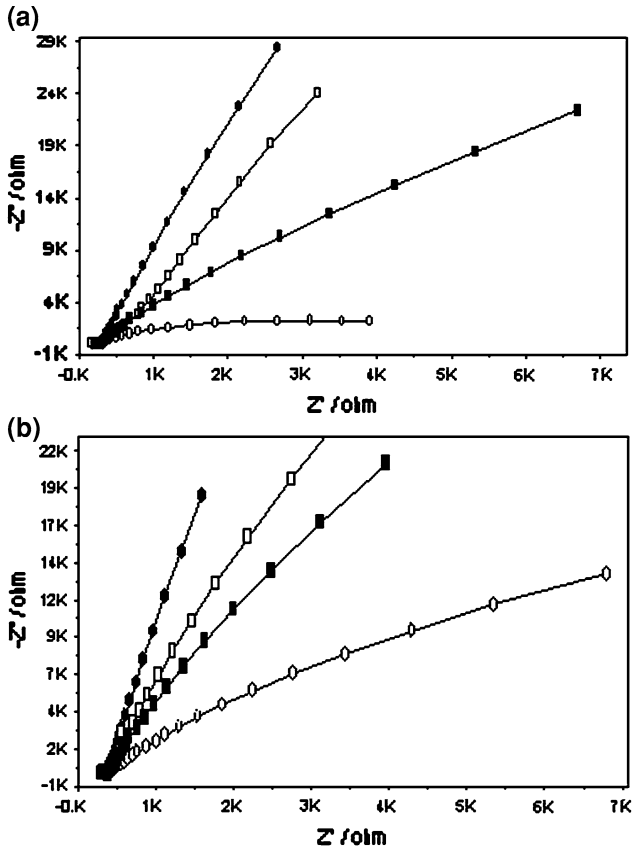

Fig. 3 (**a**) Nyquisite plots for TiO_2 and TiO_2–SiO_2 coatings on Ti (○, T.O TiO_2; ●, 100 wt.% TiO_2 + 0 wt.% SiO_2; □, 90 wt.% TiO_2 + 10 wt.% SiO_2; ■, 80 wt.% TiO_2 + 20 wt.% SiO_2 in (**a**) 0.9% NaCl and (**b**) HBSS at pH 7.4 and 25°C

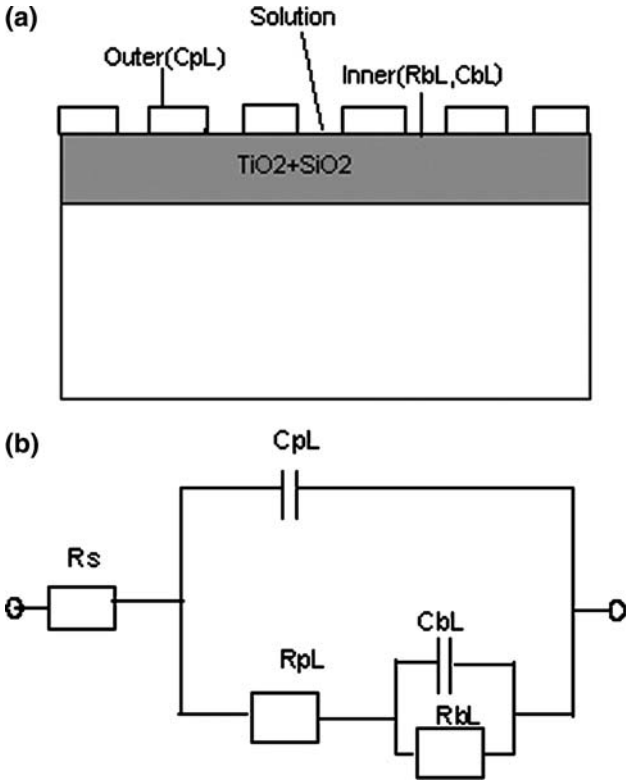

Fig. 4 (a) Two-layer model for the TiO_2 and TiO_2–SiO_2 coatings on Ti, (**b**) Equivalent circuit fitting the impedance spectra for the TiO_2 and TiO_2–SiO_2 coatings

Table 2 The electrochemical impedance parameters

S. no.	Wt.% of TiO_2–SiO_2 on Ti substrate	R_s Ohm	R_p Ohm	CPE nF	*n*
0.9% NaCl					
1	T.O TiO_2	−78.64	89.76	9.01	1.25
2	100 wt.% TiO_2 + 0 wt.% SiO_2	−75.82	92.38	9.30	1.26
3	90 wt.% TiO_2 + 10 wt.% SiO_2	−207.19	247.88	152	0.60
4	80 wt.% TiO_2 + 20 wt.% SiO_2	−77.29	91.94	9.57	1.26
HBSS					
1	T.O TiO_2	−76.46	92.42	9.44	1.26
2	100 wt.% TiO_2 + 0 wt.% SiO_2	−78.05	91.52	9.36	1.25
3	90 wt.% TiO_2 + 10 wt.% SiO_2	−77.66	95.25	7.65	1.22
4	80 wt.% TiO_2 + 20 wt.% SiO_2	−74.42	89.01	9.08	1.26

exhibited a cathodic shift. The TiO_2–SiO_2 mixed oxide coating attained a maximum positive value in 4 days, the 100 wt.% TiO_2 coating by thermal decomposition in 5 days, and the TiO_2 coatings obtained by thermal oxidation in 7 days.

TF-XRD pattern of the TiO_2 coating formed by thermal treatment and the TiO_2 and TiO_2–SiO_2 mixed oxide coating formed by thermal decomposition are shown in Fig. 6. The resultant values of 2θ are compared with the standard cards of JCPDS [20]. The major phase of TiO_2 formed after firing the $TiCl_4$/isopropanol system at 500°C is anatase form. The major peaks appeared at $2\theta = 37°$, 48° and 55° are the peaks of anatase TiO_2. In the TF-XRD pattern of TiO_2–SiO_2 mixed oxide coatings, Fig. 6c shows no characteristic peak of pure SiO_2 ($2\theta = 23°$) [21]. Even though the XRD peak of SiO_2 is absent, the presence of Si–O–Si bond in the TiO_2–SiO_2 coatings is evidenced from FTIR analysis and by elemental determination of Si by EDAX. The size of the particles D_{XRD} was calculated according to Scherer equation $D_{XRD} = 0.9\lambda/B\cos\theta$, where λ is the wavelength of the radiation, θ the diffraction angle, and B the corrected half-width of the diffraction peak [22]. The particle size of the TiO_2 formed by thermal decomposition is in the nanometer range, i.e., 11 nm. The TF-XRD pattern of the TiO_2 coating formed by thermal oxidation and the 100 wt.% TiO_2 and the TiO_2–SiO_2 mixed oxide coatings formed by thermal decomposition recorded after alkaline treatment and soaking in 1.5 SBF are shown in Fig. 7. All

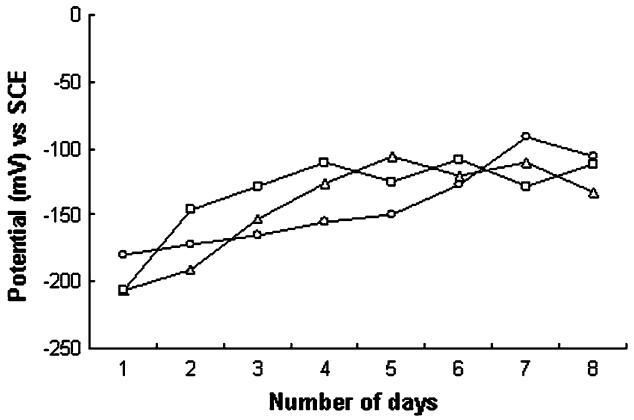

Fig. 5 Surface potential change on the TiO_2 and TiO_2–SiO_2 coatings during biomimetic growth (○, T.O TiO_2; △, 100 wt.% TiO_2 + 0 wt.% SiO_2; □, 90 wt.% TiO_2 + 10 wt.% SiO_2) in 1.5 SBF at pH 7.4 and 36.5°C

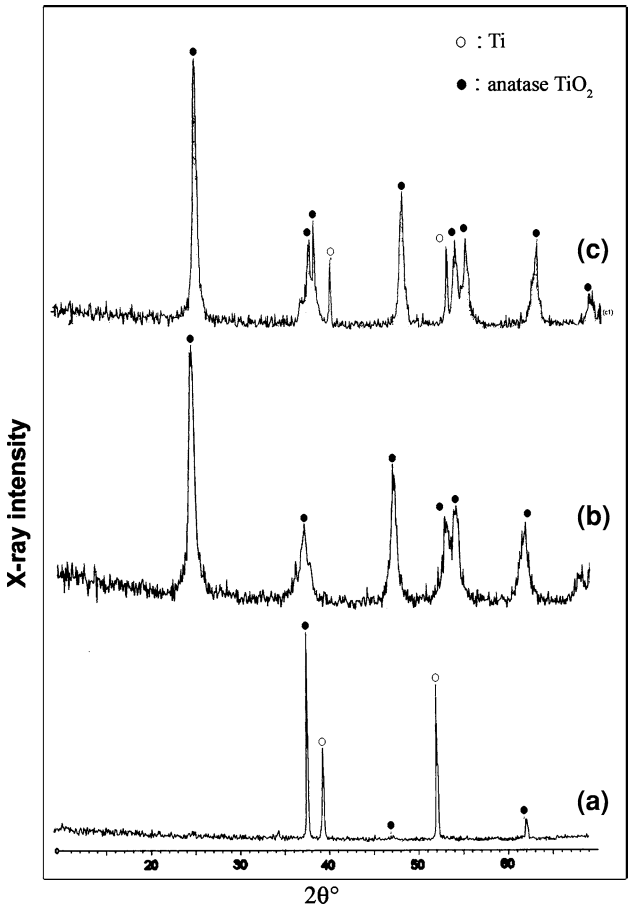

Fig. 6 TF-XRD pattern of (**a**) T.O TiO_2 (**b**) 100 wt.% TiO_2 + 0 wt.% SiO_2 and (**c**) 90 wt.% TiO_2 + 10 wt.% SiO_2 coatings on Ti

the coatings show characteristic peaks of apatite and peaks appeared at $2\theta = 25°$, 40°, 45°, and 55°.

The FTIR spectrum of the TiO_2 coating formed by thermal oxidation and the 100 wt.% TiO_2 and TiO_2–SiO_2 mixed oxide coatings formed by thermal decomposition before and after soaking in 1.5 SBF are shown in Fig. 8. In the FTIR spectrum of TiO_2–SiO_2 mixed oxide coatings, in addition to the peaks obtained for TiO_2 coatings, it show a band at 1,109 cm^{-1} due to asymmetrical vibration of the Si–O–Si bond in the tetrahedral SiO_4 unit of the TiO_2–SiO_2 coatings. The symmetrical Si–O–Si stretching vibration appeared at 815 cm^{-1}. The band at 476.21 $cm^{-1}$is due to vibrational mode of bending of Si–O–Si [23, 24]. The TiO_2 and TiO_2–SiO_2 coating after soaking in 1.5 SBF show peaks at 596 cm^{-1} due to PO_4^{3-} bending vibrational mode. Peaks at 905.39 and 909.3 were due to P–O stretching in HPO_4^{2-}. The coatings show peaks at 1,036 cm^{-1} also due to P–O stretching in PO_4^{3-}. The peaks around 1,552 and 1,632 cm^{-1} are due to C–O stretching vibration [25]. The peaks at 3,199 and 3,227 cm^{-1} are due to O–H stretching vibration [26].

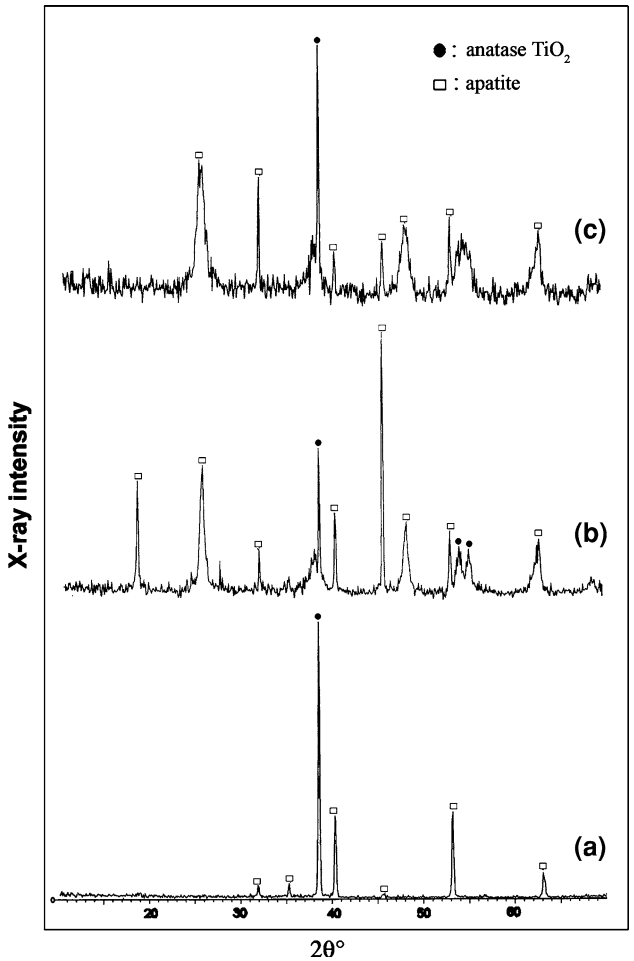

Fig. 7 TF-XRD pattern of (**a**) T.O TiO_2 (**b**) 100 wt.% TiO_2 + 0 wt.% SiO_2 and (**c**) 90 wt.% TiO_2 + 10 wt.% SiO_2 coatings after alkaline treatment and soaking in 1.5 SBF at pH 7.4 and 36.5°C for 7 days

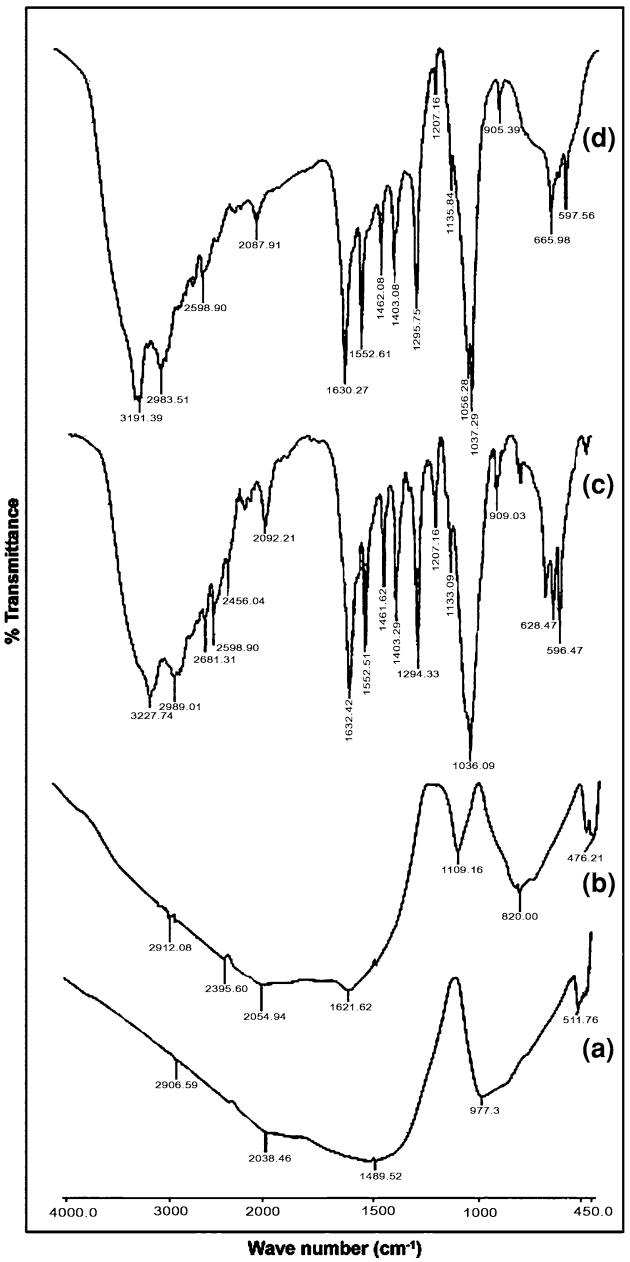

Fig. 8 FTIR spectrum of (**a**) 100 wt.% TiO_2 + 0 wt.% SiO_2 and (**b**) 90 wt.% TiO_2 + 10 wt.% SiO_2 coatings, (**c**) 100 wt.% TiO_2 + 0 wt.% SiO_2, and (**d**) 90 wt.% TiO_2 + 10 wt.% SiO_2 coatings after alkaline treatment and soaking in 1.5 SBF at pH 7.4 and 36.5°C for 7 days

The SEM micrograph and associated EDAX pattern of the TiO_2 coating formed by thermal oxidation, the 100 wt.% TiO_2 and 90 wt.% TiO_2–10 wt.% SiO_2 mixed oxide coatings formed by thermal decomposition are shown in Fig. 9. The TiO_2 and TiO_2–SiO_2 coatings formed by thermal decomposition are much denser than the TiO_2 coatings formed by thermal oxidation. In the micrograph of the TiO_2–SiO_2 mixed oxide coating white globular masses appeared on the surface which could be attributed to the SiO_2 particles. The cracks and grooves appeared on the TiO_2 and TiO_2–SiO_2 mixed oxide coatings obtained by thermal decomposition may be due to the contracting forces in the drying process of $TiCl_4$/isopropanol system [27]. There was no much distinction that could be arrived from the micrograph of the 80 wt.% TiO_2–20 wt.% SiO_2 with respect to 90wt.% TiO_2–10 wt.% SiO_2. Figure 10 shows the SEM micrograph and associated EDAX pattern of the coatings after alkaline treatment and soaking in 1.5 SBF. After bio-growth study white precipitates were observed on the surface of TiO_2 and TiO_2–SiO_2 mixed oxide coatings, revealing the presence of apatite. The apatite phase was confirmed by structural and crystallographic analysis by FTIR and TF-XRD. The apatite was found to be grown more on the surface of TiO_2–SiO_2 mixed oxide coating than the TiO_2 coatings obtained by thermal oxidation and decomposition methods. It was also evidenced from the elemental analysis of Ca and P in 1.5 SBF by ICP-AES and spectrophotometry. Table 3 shows the ICP-AES and spectrophotometric results of Ca and P in the Kokubo's 1.5 SBF solution after soaking the specimens for 7 days. The Ca and P content of the SBF solution decreased after bio-growth study. The decrease was more pronounced for the SBF solution obtained by the soaking of TiO_2–SiO_2 coated specimens, i.e., a decrease from Ca: 163.6 ppm → 77.7 ppm; P: 73 ppm → 59.7 ppm. This depletion was due to more precipitation of apatite on the surface of the TiO_2–SiO_2 coatings, which was further confirmed by the EDAX results as shown in Table 4. The elemental % of Ca and P on the surface of TiO_2–SiO_2 coatings was higher than the 100 wt.% TiO_2 coatings obtained by thermal decomposition which was still higher than the TiO_2 coatings obtained by thermal oxidation.

4 Discussions

4.1 Surface characterization

A nanosized anatase TiO_2 particles-containing coating was developed by thermal decomposition of $TiCl_4$/isopropanol on Ti at 500°C. The mechanism of the thermal decomposition of $TiCl_4$/isopropanol has been already reported [12]. When mixed with isopropanol, $TiCl_4$ reacts with isopropanol to form $TiCl_x(OCH(CH_3)_2)_{4-x}$ species and HCl gas. $TiCl_x(OCH(CH_3)_2)_{4-x}$ species absorbs water from atmosphere to form $Ti(OH)_4$ precursor, which is polymerized to be an inorganic polymer layer on Ti. Anatase TiO_2 powder forms after the precursor is fired at 500°C for 1 h. When small wt.% of SiO_2 powder in pure form is added it may get dispersed in the $TiCl_4$/isopropanol system. When fired at 500°C a uniform TiO_2–SiO_2 coating layer is obtained. The Vickers microhardness values tend to decrease with

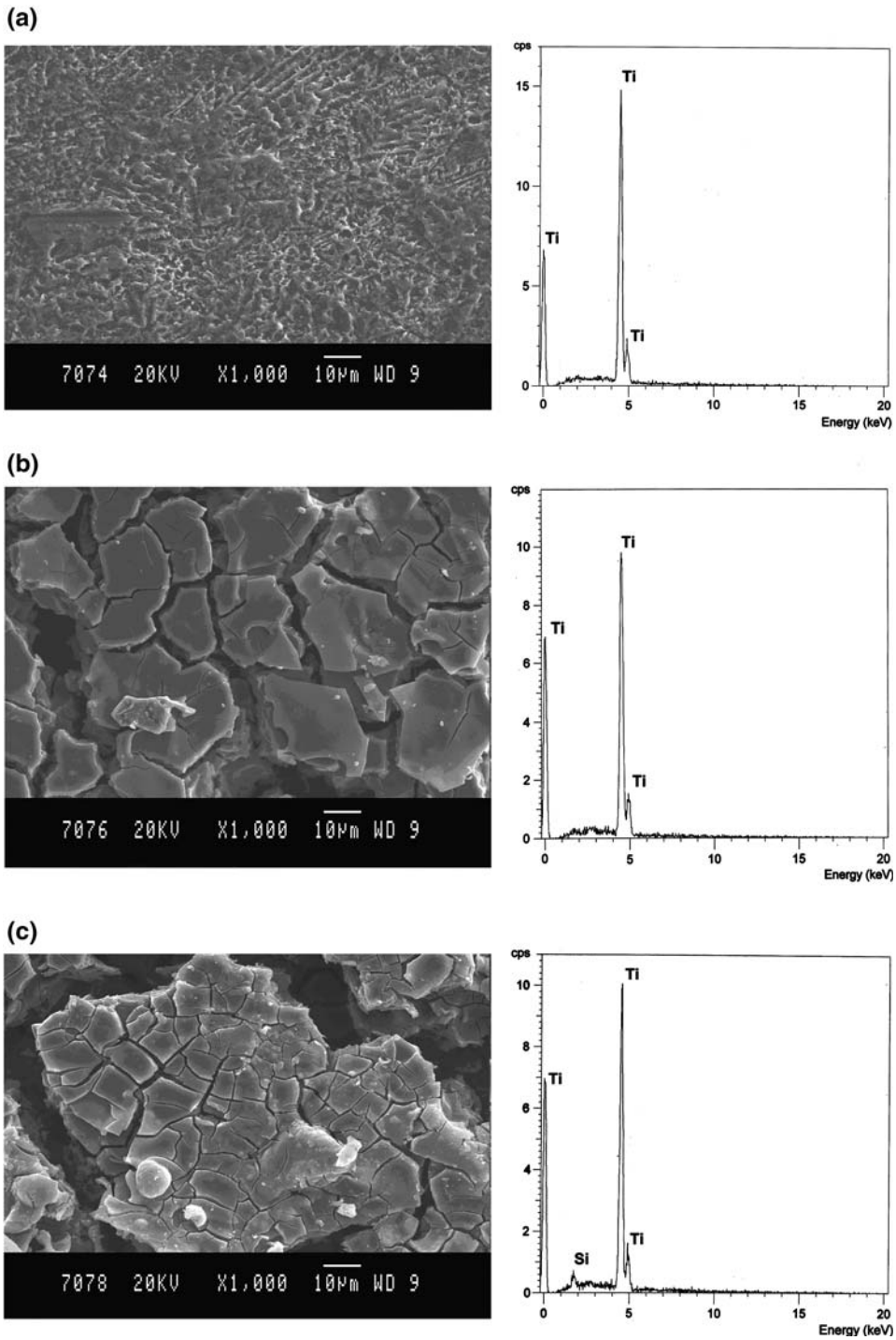

Fig. 9 SEM micrograph and associated EDAX pattern of (**a**) T.O TiO_2 (**b**) 100 wt.% TiO_2 + 0 wt.% SiO_2, and (**c**) 90 wt.% TiO_2 + 10 wt.% SiO_2 coatings on Ti

increase in wt.% of SiO_2. The adhesion and wear resistance of the TiO_2–SiO_2 mixed oxide coating containing optimum wt.% of TiO_2 and SiO_2, i.e., 90 wt.% TiO_2 + 10 wt.% SiO_2 was higher than that of the pure TiO_2 coatings, which revealed high stability of the TiO_2–SiO_2 coatings. These nanostructured TiO_2 and TiO_2–SiO_2 coatings were composed of sufficient small particles and are highly porous in nature.

4.2 Electrochemical evaluation

All the TiO_2 coatings and the TiO_2–SiO_2 coatings exhibited a cathodic potential shift initially in both 0.9% NaCl and HBSS, due to the porous nature of the coatings. The nanosized TiO_2–SiO_2 coatings formed by thermal decomposition method had enough pores at the surface. After few days the surface became passive in both the physiological

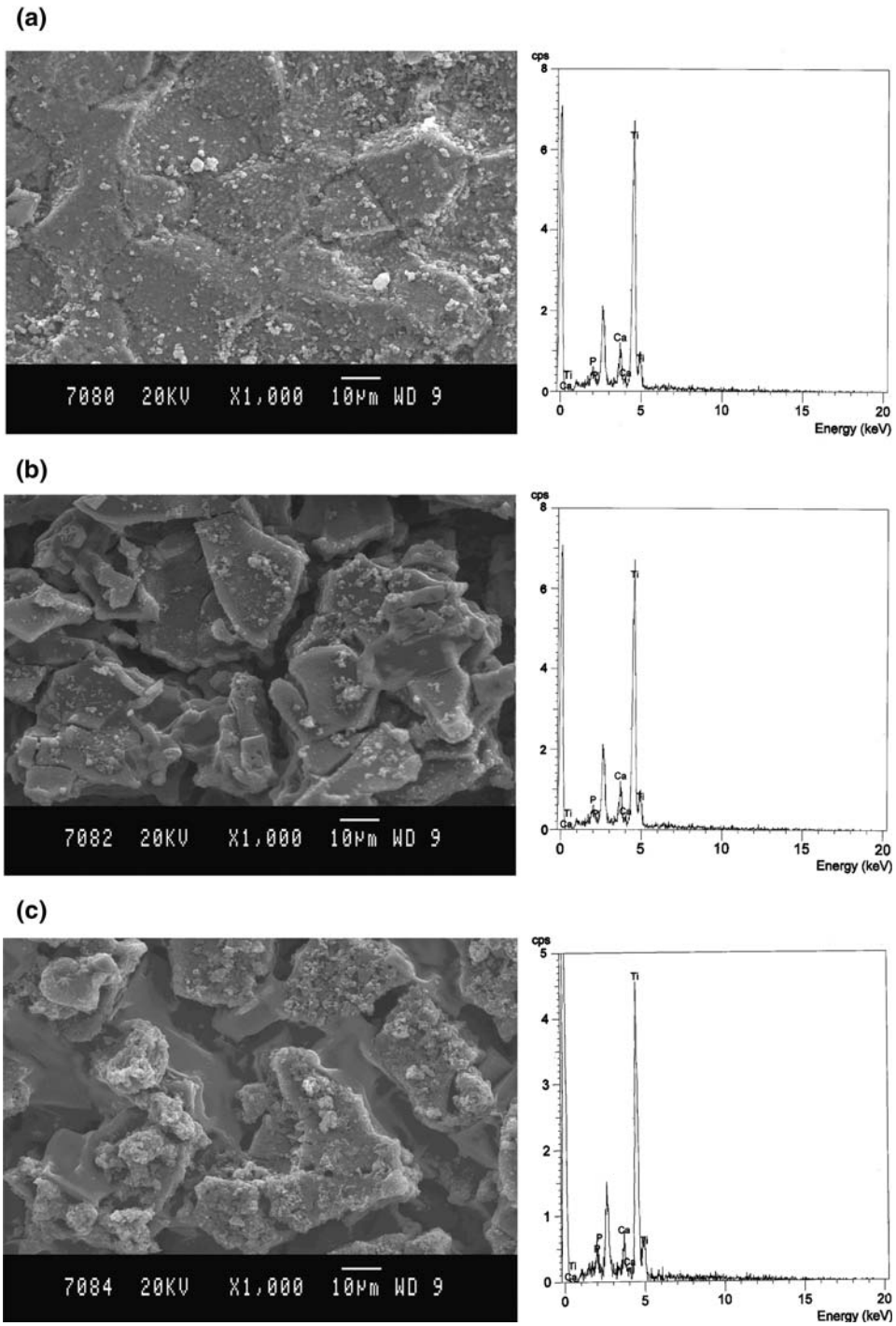

Fig. 10 SEM micrograph and associated EDAX pattern of (**a**) T.O TiO_2 (**b**) 100 wt.% TiO_2 + 0 wt.% SiO_2 and (**c**) 90 wt.% TiO_2 + 10 wt.% SiO_2 coatings on Ti after alkaline treatment and soaking in 1.5 SBF at pH 7.4 and 36.5°C for 7 days

Table 3 ICP-AES/spectrophotometric results of 1.5 SBF after biomimetic growth for 7 days

Specimen soaked in 1.5 SBF	Element concentration (ppm)	
	Calcium	Phosphorus
T.O TiO_2	93.7	72.3
100 wt.% TiO_2 + 0 wt.% SiO_2	80.5	52.5
90 wt.% TiO_2 + 10 wt.% SiO_2	77.7	59.7

Table 4 Elemental determination of HAp coatings by EDAX

Specimen soaked in 1.5 SBF	Elemental %		Ca/P ratio
	Calcium	Phosphorus	
T.O TiO_2	1.05	0.88	1.19
100 wt.% TiO_2 + 0 wt.% SiO_2	7.48	3.66	2.04
90 wt.% TiO_2 + 10 wt.% SiO_2	7.58	4.49	1.68

solutions and hence a steady potential was reached. The TiO_2–SiO_2 coating containing the optimum wt.% of TiO_2 and SiO_2, i.e., 90 wt.% TiO_2 + 10 wt.% SiO_2 was least cathodic, which showed the least corrosive tendency and high stability of the coatings.

A network of polymeric oxides was formed by thermal decomposition of $TiCl_4$/isopropanol system. These TiO_2 and TiO_2–SiO_2 coatings were sufficiently thick and possessed high adhesive strength on the Ti metal substrate. This revealed why the TiO_2 and TiO_2–SiO_2 coating layers could withstand at high current density during anodic polarization.

In the Nyquisite plot of the TiO_2 and TiO_2–SiO_2 coated specimens, the inductance was recorded at the end of the first semi-circle of the high-frequency region. Da Silva et al. interpreted the main cause of such inductive behavior to the disorderly movement of charge carriers through the complex microstructures comprising pores, cracks, grain boundaries, etc., of the metal oxides-incorporated matrix [28]. The two-layer model of the oxide film as shown in Fig. 4a, was well supported by EIS results obtained. R_{bL} obtained for all the oxide coatings were found to be greater than R_{pL} and are obtained in kOhm, showing that the resistance of the oxide coating on Ti is due to this barrier layer. In both the 0.9% NaCl and HBSS solutions, R_{bL} value obtained for 90 wt.% TiO_2 + 10 wt.% SiO_2 coatings on Ti was found to be higher than the 100 wt.% TiO_2 coating formed by thermal decomposition. For the same coating R_{pL} decreased and C_{pL} increased than that of the 100 wt.% TiO_2 coating. It is generally accepted that the pores in the outer layer may be filled with electrolyte, and this might have contributed to the larger values of C_{pL} comparatively to C_{bL}. While corrosion resistance of the substrate is ascribed to the barrier layer, its good ability to osteointegrate can be attributed to the presence of the porous layer. The low current density displayed by the TiO_2–SiO_2 coatings under high applied potential may be due to this thick inner barrier layer, while its outer porous layer may be one of the reasons for high biomimetic growth rate which could facilitate further osteointegration.

4.3 Evaluation of bioactivity

The bioactivity of both the sol–gel derived TiO_2 and SiO_2 has been well established, they have their IEPs below the physiological at pH 7.4 (for silica near 2 and for titania near 6) [29]. The TiO_2–SiO_2 coatings were found to be more bioactive than 100 wt.% TiO_2 coatings formed by thermal decomposition. Since the IEP of silica is 2, the surface of the TiO_2–SiO_2 coating became comparatively highly negative and hence attracted the positively charged Ca^{2+} ions and then PO_4^{3-} groups in the SBF favoring apatite growth. TF-XRD studies revealed that the major phase of TiO_2 in the coating was anatase. The crystallographic matching between the anatase TiO_2 and apatite crystal plane also favored apatite growth in SBF. The Ca/P ratio obtained for the apatite grown over the TiO_2–SiO_2 coating is 1.68, close to that of natural bone apatite [30]. However, there was least apatite growth on the TiO_2 coating formed by thermal oxidation as the coating was thin and had low number of nucleation sites favoring biogrowth. The TiO_2/TiO_2–SiO_2 coatings formed by thermal decomposition had much more porous outer layer (from EIS results) and facilitated ion exchange with the SBF solution favoring effective apatite growth. These nanosized negatively charged nucleation sites could favor apatite growth in natural biomimetic system.

The surface activation of TiO_2 and SiO_2 was achieved by alkaline treatment in 5 M NaOH at 60°C for 24 h [31]. It has been found that the surface treated TiO_2–SiO_2 coatings formed sodium titanate ($Na_2Ti_5O_{11}$) and sodium silicate (Na_2SiO_4) layer. These sodium titanate and sodium silicate could form many more Si–OH and Ti–OH groups in SBF. The mechanism of apatite formation on TiO_2 and SiO_2 in SBF can be interpreted in terms of the electrostatic interaction of the surface oxide with the ions in the fluid. When exposed to SBF, the Na^+ ions in the surface layer of $Na_2Ti_5O_{11}$ and Na_2SiO_4 exchanged with H_3O^+ions present in the fluid facilitating the formation of Ti–OH and Si–OH groups. The surface potential analysis of TiO_2 and TiO_2–SiO_2 coatings (Fig. 5) showed that the surface potential was highly negative due to the formation of Ti–OH and Si–OH groups on the surface of the coating. The negatively charged Ti–OH and Si–OH groups combined selectively with positively charged Ca^{2+} ions in the fluid leading the surface gradually to gain overall positive surface potential and finally it attained a maximum value. The positively charged surface combined with the negatively charged phosphate ions to form an amorphous Ca–P and the potential shifted in negative direction. This Ca–P spontaneously transformed into crystalline apatite [32]. The HAp is known to reveal a negative charge in the body environment because of the hydroxyl and phosphate groups on its surface [33]. Once formed, the apatite grows spontaneously by taking calcium and phosphate ions in the fluid [34, 35].

5 Conclusions

The process developed for the coating of Ti with nanosized titania particles having anatase structure by thermal decomposition of $TiCl_4$ was found to be reliable and reproducible. Hardness of the TiO_2–SiO_2 mixed oxide coatings tend to decrease with increasing in SiO_2 content. The adhesion and wear resistance of the TiO_2–SiO_2 coating

containing optimum wt.% of TiO_2 and SiO_2 were improved when compared with that of the 100 wt.% TiO_2 coating. The TiO_2–SiO_2 mixed oxide coatings were highly porous in nature. The electrochemical evaluation by anodic polarization and EIS analysis revealed that the TiO_2 and the TiO_2–SiO_2 coatings formed by thermal decomposition had a stable and compact inner layer having high resistance to corrosion. Enhanced bioactivity was achieved by the incorporation of SiO_2 in the TiO_2 and TiO_2–SiO_2 coatings. Their bioactivity was attributed to (1) nanostructured surface composed of enough small particles which is required for the formation of carbonate containing apatite, (2) crystallographic matching between the anatase TiO_2 and the apatite crystal plane, (3) the existence of abundant OH^- groups on the surface in SBF, and (4) both titania and silica have their IEPs below the physiological pH 7.4 and facilitating negatively charged surface in body fluid. The high stability and enhanced bio-growth on the coating revealed the effective applications of the coating for orthopaedic implants.

References

1. N. Moritz, S. Areva, J. Wolke, T. Peltola, Biomaterials **26**, 4460 (2005)
2. S. Lin, R.Z.L. Geros, J.P.L. Geros, J. Biomed. Mater. Res. **66A**, 819 (2003)
3. X. Zhu, J. Chen, L. Sceideler, R. Reichl, J. Geis-Gerstorfer, Biomaterials **25**, 4087 (2004)
4. D.F. William (ed.), *Titanium and Titanium Alloys*, vol. 1. (CRC Press, Inc., Boca Raton FL, 1981), p. 9
5. Q. Liu, J. Ding, F.K. Mante, S.L. Wunder, G.R. Baran, Biomaterials **23**, 3103 (2002)
6. A. Bigi, E. Boanini, B. Barbara, A. Facchini, S. Panzavolta, F. Segatti, L. Sturba, Biomaterials **26**, 4085 (2005)
7. H. Ishizawa, M. Ogino, J. Biomed. Mater. Res. **29**, 1071 (1995)
8. S. Areva, V. Aaritalo, S. Tuusa, M. Jokinen, M. Linden, T. Peltola, J. Mater. Sci. Mater. Med. **18**, 1633 (2007)
9. M. Shirkhanzadeh, J. Mater. Sci. Mater. Med. **3**, 322 (1992)
10. F. Brossa, B. Looman, R. Dietra, E. Sabbioni, M. Gallorini, E. Orvini, in *High Tech Ceramics*, ed. by P. Vincenzinia (Elsevier, Amsterdam, 1987), p. 99
11. C.M. Lin, S.K. Yen, J. Mater. Sci. Mater. Med. **16**, 889 (2005)
12. Y. Zhu, L. Zhang, C. Gao, L. Cao, J. Mater. Sci. Mater. Med. **35**, 4049 (2000)
13. J. Wang, P. Layrolle, M. Stigter, K. De Groot, Biomaterials **25**, 583 (2004)
14. S.M.A. Shibli, V.S. Saji, Corros. Sci. **47**, 2213 (2005)
15. F. Barrere, P. Layrolle, C.A.V. Blitterswijk, K. De Groot, Biomaterials **23**, 2211 (2002)
16. F. Barrere, C.A.V. Blitterswijk, K. De Groot, P. Layrolle, Mater. Res. Soc. Symp. Proc. **599**, 135 (2000)
17. C.M. De Assis, L.C.O. De Vercik, M.L. Dos Santos, M.V.L. Fook, A.C. Guastaldi, Mater. Res. **8**, 207 (2005)
18. L. Jonasova, F.A. Muller, J.S. Helebrant, P. Greil, Biomaterials **23**, 3095 (2002)
19. I.C. Lavos-Valerreto, S. Wolynec, I. Ramires, A.C. Guastaldi, I. Costa, J. Mater. Sci. Mater. Med. **15**, 55 (2004)
20. JCPDS International Centre for Diffraction Data, Powder Diffraction File (Swarthmore, PA, 1980)
21. F. Chiker, J.P.H. Nogier, F. Launay, J.L. Bonardet, Appl. Catal. A **243**, 309 (2003)
22. Y.P. Fer, C.H. Lin, C.S. Hsu, J. Alloys Compd **391**, 110 (2005)
23. D. Sun, Y. Huang, B. Han, G. Yang, Langmuir **22**, 4793 (2006)
24. I. Barba, A.J. Salinas, M.V. Regi, J. Biomed. Mater. Res. **47**, 243 (1997)
25. F. Barrere, C.M.V.D. Valk, D. Raj, C.A.V. Blitterswijk, K. De Groot, P. Layrolle, J. Biomed. Mater. Res. **64A**, 378 (2003)
26. S.N. Boon, I. Annergren, A.M. Soutar, K.A. Khor, A.E.W. Jarfors, Biomaterials **26**, 1087 (2005)
27. H.B. Wen, J.R. De Wijn, F.Z. Cui, K. De Groot, Biomaterials **19**, 215 (1998)
28. L.M.D. Silva, K.C. Fernades, L.A.D. Faria, J.F.C. Boodts, Electrochim. Acta **49**, 4893 (2004)
29. P. Li, C. Ohtsuki, T. Kokubo, K. Nakanishi, N. Soga, K. De Groot, J. Biomed. Mater. Res. **28**, 7 (1994)
30. Y. Man, K. Xu, J. Lu, J. Mater. Sci. Mater. Med. **35**, 4049 (2000)
31. H.M. Kim, T. Himeno, M. Kawashita, J.H. Lee, T. Kokubo, T. Nakamura, J. Biomed. Mater. Res. **67A**, 1305 (2003)
32. H. Takadama, H.M. Kim, T. Kokubo, T. Nakamura, J. Biomed. Mater. Res. **55**, 185 (2001)
33. P. Somasundaran B. Markovic, in *Interfacial Properties of Calcium Phosphate*, ed. by Z. Amjad (Tran Tech Publications, Ae dermannsdor, Switzerland, 1998), p. 85
34. W. Neuman, M. Neuman, *The Chemical Dynamics of Bone Mineral* (University of Chicago Press, Chicago, 1958)
35. J. Gamble, *Chemical Anatomy, Physiology and Pathology of Extracellular Fluid* (Harvard University Press, Cambridge, MA, 1967)